Sadia Asad · Shehnila Riaz

Analysis of entropy generation and nonlinear convection on unsteady flow of MHD Prandtl fluid with Soret and Dufour effects

Abstract Here the assessment of entropy generation with Soret and Dufour impact in flow of MHD Prandtl fluid along an unsteady stretching surface has been measured. Nonlinear mixed convection and convective conditions for heat/mass transfer are imposed at the surface. The outcome of viscous dissipation and radiation is considered in heat transfer features. The obtained system of nonlinear PDEs is converted to ODEs by consuming dimensionless variables. Resulting systems are solved for the convergent solutions. Impacts of Prandtl fluid parameters, unsteadiness parameter, Soret and Dufour numbers, magnetic parameter, nonlinear thermal and concentration parameter, Prandtl number, radiation parameter, thermal and concentration Biot numbers, ratio of concentration to thermal buoyancy, Eckert number and Schmidt number are addressed. Skin friction coefficient, local Nusselt and Sherwood numbers are analyzed graphically. Unsteady parameter ϵ has reverse behavior on the velocity and temperature profiles, velocity declines while temperature raises. Prandtl fluid parameter α and β boost the velocity field. Mixed convection parameter le and N^* (ratio of concentration and buoyancy force) enhance the velocity field and resultant boundary layer thickness. Magnetic parameter change its behavior on $f(\eta)$ $\theta(\eta)$ and . Soret/Dufour number enhances the energy flux due to mass transfer rate and mass flux which radically increases the temperature. Far away from the wall entropy generation grows rapidly for greater values of a and b. Magnetic and radiation parameter increase the entropy generation while radiation parameter decreases.

Mathematics Subject Classification   76A02 · 76A05

List of symbols

u, v	Velocity components
x, y	Space coordinates
σ	Stefan–Boltzmann constant
g	Gravitational acceleration
T	Fluid temperature
T_∞	Ambient temperature
C	Fluid concentration
C_∞	Ambient concentration
A and $\bar{C}$	Material constant of Prandtl fluid
$U_w(x, t)$	Stretching velocity
u_∞	Free stream velocity

S. Asad (✉)
Department of Mathematics, College of Science, Majmaah University, Al-Majmaah 11952, Saudi Arabia
E-mail: sadia.k@mu.edu.sa

S. Riaz
Department of Mathematics, Quaid-i-Azam University, 45320 Islamabad, Pakistan

ρ	Fluid density
ν	Kinematic viscosity
μ	Dynamic viscosity
c_p	Specific heat
σ	Electrical conductivity
β_T	Thermal expansion coefficient
β_C	Concentration expansion coefficient
ρ_f	Fluid density
$(c_p)_f$	Fluid heat capacity
Bi_1	Thermal Biot number,
Bi_2	Concentration Biot number
q_r	Radiative heat flux
Ω_1	Linear thermal expansion coefficients
Ω_2	Nonlinear thermal expansion coefficients
Ω_3	Linear concentration expansion coefficients
Ω_4	Nonlinear concentration expansion coefficients
σ^*	Stefan–Boltzmann constant
k^*	Mean absorption coefficient
η	Dimensionless space variable
f	Dimensionless velocity
θ	Dimensionless temperature
ϕ	Dimensionless concentration
ψ	Stream function
α and β	Prandtl fluid parameters
M	Magnetic parameter
k_T	Thermal diffusion ratio
λ	Mixed convection
N^*	Ratio of buoyancy forces
R	Radiation parameter
Pr	Prandtl number
N_b	Brownian motion
N_t	Thermophoresis variable
ϵ	Unsteadiness parameter
Du	Dufour number
Sr	Soret number

1 Introduction

Unsteady flow over a stretching surface has been widely used in annealing and thinning of copper wires, paper production sheet from a dye, metals, and plastics, cooling of the metallic plate in a cooling bath, glass blowing and food processing. Boundary layer flow and heat transfer over a permeable unsteady stretching sheet with non-uniform heat source/sink is examined by Zheng et al. [34]. Unsteady boundary layer stagnation-point flow over a shrinking stretching surface has been reported by Bhattacharyya [9]. He considered that the sheet temperature depends on time; also he found out dual solutions for same values of velocity ratio parameter as well as unique solution of the problem. Mukhopadhyay [24,25] reported Casson fluid flow over an unsteady stretching surface with a chemical reaction. They discuss that fluid velocity initially decreases with increasing values of time depending on parameter while temperature and concentration fields decay, because less heat and solute is moved from the sheet to fluid. Lin et al. [21] examined the flow and heat transfer of pseudoplastic nanoliquid in a finite slim film across an unsteady stretching sheet. They also considered variable thermal conductivity and viscous dissipation effects. Rosca and Pop [27] examined time dependent viscous flow across a curved stretching/shrinking surface with mass suction. They solved the dimensionless system numerically and performed stability analysis for solution. Also conclude that pressure cannot be negligible in curved surfaces. Lin et al. [22] numerically studied the magnetohydrodynamic (MHD) pseudoplastic flow of a nanofluid in a finite film over an unsteady stretching surface with internal heating effects. They consider water as base fluid with nanoparticles (Cu, Al_2O_3, CuO and TiO_2). They discussed that when time-dependent parameter goes to zero then film thickness approaches to infinity. The time-dependent 2D flow of non-Newtonian fluid across a

stretching sheet with thermal radiation and variable thermal conductivity has been evaluated by Reddy [26]. He calculated that the rate of cooling for larger values of the time dependent parameter is significantly bigger than this rate in steady flows. Unsteady flow of Powell–Eyring fluid past an inclined stretching surface was discovered by Hayat et al. [15]. They also studied the collective effects of non-uniform heat source/sink and radiation.

The combined effect of heat/mass transfer is significant in different fields including moisture over the agriculture field, distribution of temperature, cooling towers and food processing and many others. The Soret/Dufour effects are very prominent in the analysis of heat/mass transfer. Therefore Hayat et al. [12] studied the effects of Soret/Dufour in mixed convection flow towards a vertical surface. Hayat et al. [13] also discussed Soret and Dufour impacts in three-dimensional boundary layer flow of viscoelastic fluid over a stretching surface. Tsai and Huang [31] explored Soret and Dufour impacts in Hiemeng flow through a stretching sheet. Zheng et al. [35] analyzed the unsteady heat and mass transfer in MHD fluid by an oscillatory stretching surface. They consider the effect of viscous dissipation and uniform magnetic field that applied in vertical direction of the flow. They studied that at the same time when we increase Dufour number and decrease Soret number, temperature field increases while spices decays. Wang et al. [33] explained the influence of thermo-solutal buoyancies with Soret and Dufour belongings. In this study, they found that the flow composition of various aspects ratios develops from condition-controlled to steady convection-controlled and complete growth of Rayleigh number increases. Radiative heat and mass transfer flow with Soret and Dufour effects have been reported by Vedavathi et al. [32]. They solve OD Eq by using shooting method along with Runge–Kutta fourth order integration scheme. They conclude that radiation parameter enhances the velocity and temperature profile while it decays the heat transfer rate. Hayat et al. [14] explored the Soret/Dufour impacts in the MHD rotating flow of viscoelastic fluid. They model three dimension flow in the rotating frame of reference . Series solution is obtained and described that result for porous channel. The flow behavior is different for upper and lower plate.

The present communication is to analyze the entropy generation flow of non-Newtonian fluid induced over an unsteady stretching surface with Soret/Dufour effects. Constitutive relations for MHD Prandtl fluid are considered. Viscous dissipation nonlinear mixed convection and thermal radiation are also taken into account. Convective heat and mass conditions were imposed. The coupled highly nonlinear equations are solved analytically. The effects of physical parameters on the velocity, temperature and concentration profiles are deliberated. Skin friction, local Nusselt and Sherwood numbers are also discussed.

2 Problem formulation

Consider the flow of Prandtl fluid across an unsteady stretching surface with heat/mass transfer. It is assumed that the surface is stretched with two equal and opposite forces along the x-axis keeping the origin fixed. The *x*-axis is taken along the sheet and *y*-axis normal to it. Radiation, Soret/Dufour effects and viscous dissipation are deliberated. Convective heat and mass conditions are considered at the stretching sheet.
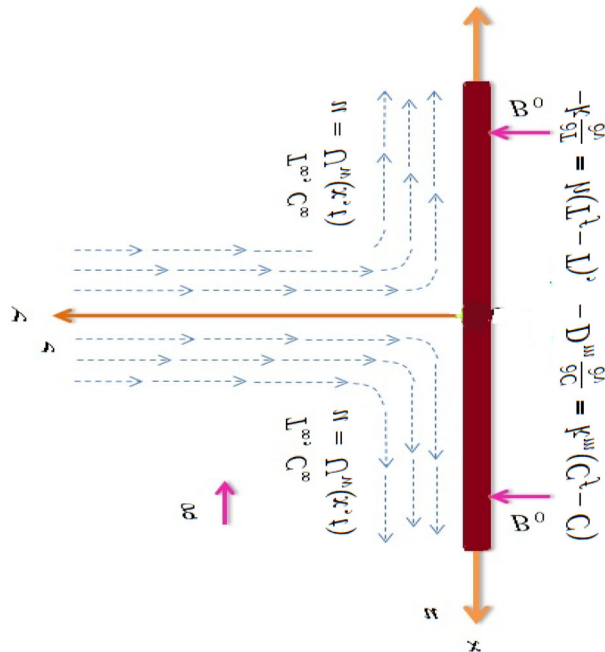

Fig. a. Flow diagram

The governing equations of the velocity, temperature and concentration fields are as follows

$$\frac{\partial u}{\partial x} + \frac{\partial v}{\partial y} = 0, \tag{1}$$

$$\frac{\partial u}{\partial t} + u\frac{\partial u}{\partial x} + v\frac{\partial u}{\partial y} = \left[\frac{A}{\rho\bar{C}}\frac{\partial^2 u}{\partial y^2} + \frac{A}{2\rho\bar{C}^3}\left(\frac{\partial u}{\partial y}\right)^2\frac{\partial^2 u}{\partial y^2}\right] - \frac{\sigma B_0}{\rho}u + g\left\{\Omega_1(T - T_\infty) + \Omega_2(T - T_\infty)^2\right\}$$
$$g\left\{\Omega_3(C - C_\infty) + \Omega_4(C - C_\infty)^2\right\}, \tag{2}$$

$$\frac{\partial T}{\partial t} + u\frac{\partial T}{\partial x} + v\frac{\partial T}{\partial y} = \alpha^*\frac{\partial^2 T}{\partial y^2} - \frac{1}{\rho c_p}\frac{\partial q_r}{\partial y} + \frac{1}{\rho c_p}\left[\frac{A}{C}\left(\frac{\partial u}{\partial y}\right)^2 + \frac{A}{6C^3}\left(\frac{\partial u}{\partial y}\right)^4\right] + \frac{D_m k_T}{c_p c_f}\frac{\partial^2 C}{\partial y^2} + \sigma B_0 u^2, \tag{3}$$

$$\frac{\partial C}{\partial t} + u\frac{\partial C}{\partial x} + v\frac{\partial C}{\partial y} = D_m\frac{\partial^2 C}{\partial y^2} + \frac{D_m k_T}{T_m}\frac{\partial^2 T}{\partial y^2}, \tag{4}$$

$$u = U_w(x, t), \ v = 0, \ -k\frac{\partial T}{\partial y} = h(T_f - T), -D_m\frac{\partial C}{\partial y} = k_m(C_f - C) \text{ at } y = 0,$$
$$u \to 0, \ T \to T_\infty, C \to C_\infty \text{ as } y \to \infty, \tag{5}$$

where u and v represent the velocity components along the x and $y-$directions respectively, $U_w(x, t) = \frac{cx}{(1-at)}$ is the stretching velocity of sheet, (where a and c are positive constants), A and $\bar{C}$ are the material constant of Prandtl fluid, $v = \frac{\mu}{\rho}$ is the kinematic viscosity, T is the fluid temperature, T_∞ is the ambient fluid temperature, C is the fluid concentration, C_∞ is the ambient fluid concentration, α^* is the thermal diffusivity, k is the thermal conductivity, Ω_1 and Ω_2 is the linear and nonlinear thermal expansion coefficients, c_p is the specific heat, $q_r = -\frac{16\sigma T_\infty^3}{3k^*}\frac{\partial T}{\partial y}$ is the radiative heat flux, k^* is the mean absorption coefficient, σ is the Stefan–Boltzmann constant, c_f is the concentration susceptibility, D_m is the molecular diffusivity of the species concentration, g is the gravitational acceleration, k_T is the thermal diffusion ratio, h is the wall heat transfer coefficient, Ω_3 and Ω_4 is the linear and nonlinear concentration expansion coefficients, k_m is the wall mass transfer coefficient, T_m is the mean fluid temperature and convective heating process is characterized by temperature T_f and concentration near the surface is C_f.

The transformations are defined as follows:

$$u = \frac{cx}{(1-at)}f'(\eta), v = -\sqrt{\frac{cv}{(1-at)}}f(\eta),$$
$$\theta(\eta) = \frac{T - T_\infty}{T_f - T_\infty}, \ \phi(\eta) = \frac{C - C_\infty}{C_f - C_\infty}, \ \eta = \sqrt{\frac{c}{v(1-at)}}y. \tag{6}$$

Now Eq. (1) is identically satisfied and Eqs. (2–5) yield

$$\alpha f''' + ff'' - f'^2 - \epsilon\left(f' + \frac{\eta}{2}f''\right) + \beta f''f''' - Mf' + \lambda(1 + \beta_t\theta)\theta + \lambda N^*(1 + \beta_c\phi)\phi = 0, \tag{7}$$

$$\left(1 + \frac{4}{3}R\right)\theta'' + \Pr\left(f\theta' - \lambda\frac{\eta}{2}\theta'\right) + \Pr Du\phi'' + \Pr Ec\left(\alpha f''^2 + \frac{\beta}{3}f''^4\right) + \Pr EcMf'^2 = 0, \tag{8}$$

$$\phi'' + ScSr\theta'' + Sc\left(f\phi' - \lambda\frac{\eta}{2}\phi'\right) = 0, \tag{9}$$

$$f = 0, f' = 1, \ \theta'(0) = -Bi_1(1 - \theta(0)), \ \phi'(0) = -Bi_2(1 - \phi(0)) \text{ at } \eta = 0,$$
$$f' = 0, \ \theta = 0, \ \phi = 0 \text{ at } \eta = \infty, \tag{10}$$

where ϵ is the unsteadiness parameter, α and β are the Prandtl fluid parameters, Pr is the Prandtl number, Du is the Dufour number, Sr is the Soret number, λ is the mixed convection parameter, N^* is the ratio of concentration to thermal buoyancy forces, Sc is the Schmidt number, β_t and β_c is the nonlinear thermal and concentration parameters, M is the magnetic parameter, Ec is the Eckert number, Bi_1 is the thermal Biot number, Bi_2 is the

concentration Biot number and R is the radiation parameter. The definitions of these parameters are

$$\epsilon = \frac{a}{c}, \quad \alpha = \frac{A}{\mu\bar{C}}, \quad M = \frac{\sigma B_0}{\rho c}, \quad \beta = x^2 \frac{c^3}{v(1-at^3)},$$

$$\Pr = \frac{v}{\alpha^*}, \quad Sr = \frac{D_m k_T (T_f - T_\infty)}{v T_m (C_f - C_\infty)}, \quad Ec = \frac{U_w^2(x)}{c_p (T_f - T_\infty)},$$

$$Sc = \frac{v}{D_m}, \quad Bi_1 = \frac{h}{k}\sqrt{\frac{v(1-at)}{c}}, \quad Du = \frac{D_m k_T (C_f - C_\infty)}{v c_\rho c_f (T_f - T_\infty)},$$

$$R = \frac{4\sigma T_\infty^3}{kk^*}, \quad Bi_2 = \frac{k_m}{D_m}\sqrt{\frac{v(1-at)}{c}}. \qquad \lambda = \frac{Gr}{Re_x^2} \tag{11}$$

The physical quantities of interest are the skin-friction coefficient C_{f_x}, local Nusselt number Nu_x and local Sherwood number Sh_x. These are defined by

$$C_{f_x} = \frac{2\tau_w}{\rho U_w^2}, \quad \tau_w = \frac{A}{\bar{C}}\frac{\partial u}{\partial y} + \frac{A}{6\bar{C}^3}\left(\frac{\partial u}{\partial y}\right)^3 \Bigg|_{y=0}, \tag{12}$$

$$Nu_x = \frac{xq_w}{k(T_f - T_\infty)}, \quad q_w = -k\frac{\partial T}{\partial y} - \frac{16\sigma T_\infty^3}{3k^*}\frac{\partial T}{\partial y}\Bigg|_{y=0}, \tag{13}$$

$$Sh_x = \frac{J_w x}{D_m (C_f - C_\infty)}, \quad J_w = -D_m \frac{\partial C}{\partial y}\Bigg|_{y=0}, \tag{14}$$

where τ_w is the local wall shear stress and q_w is the surface heat flux. Above equations in dimensionless variables yield

$$\frac{1}{2}C_{f_x}Re_x^{1/2} = \left(\alpha f''(0) + \frac{\beta}{3}f''^3(0)\right), \tag{15}$$

$$Nu_x / Re_x^{1/2} = -\left(1 + \frac{4}{3}R\right)\theta'(0), \tag{16}$$

$$Sh_x / Re_x^{1/2} = -\phi'(0), \tag{17}$$

in which $Re_x = \frac{U_w(x,t)x}{v}$ is the local Reynolds number.

3 Convergence analysis

Convergence of constructed series solutions clearly depends upon the h_f, h_θ and h_ϕ. Therefore we plot $h-$curves for the velocity, temperature and concentration fields. Figures 1, 2, 3 depict the $h -$ curves of $f''(0)$, $\theta'(0)$ and $\phi'(0)$ for different values of involved physical parameters. Here admissible ranges of h_f, h_θ and
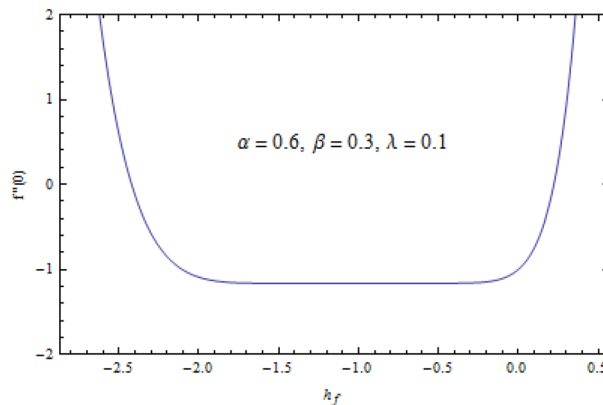
Fig. 1 $\hbar_f -$ curve for velocity field
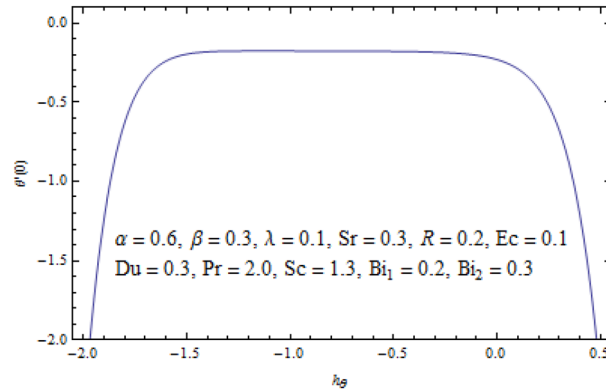
Fig. 2 $\hbar_\theta -$ curve for temperature field
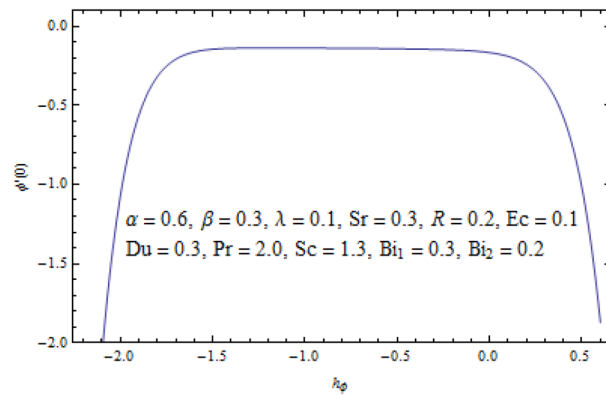
Fig. 3 $\hbar_\phi -$ curve for concentration field

Table 1 Convergence of series solutions for different order of approximations

Order of approximations	$-f''(0)$	$-\theta'(0)$	$-\phi'(0)$
1	1.1625	0.1957	0.1540
5	1.1626	0.1787	0.1438
10	1.1628	0.1768	0.1392
15	1.1628	0.1761	0.1375
20	1.1628	0.1758	0.1369
25	1.1628	0.1757	0.1366
30	1.1628	0.1756	0.1365
35	1.1628	0.1756	0.1365
40	1.1628	0.1756	0.1365

h_ϕ are $-1.8 < h_f < -0.1$, $-1.5 < h_\theta < -0.1$ and $-1.6 < h_\phi < -0.1$ respectively. Obviously the series solutions converge in the whole region of η when $h_f = -1$, $h_\theta = -9$ and $h_\phi = -8$. Table 1 ensures the convergence of HAM solutions for different order of approximations. Here the 25th-order of approximations are sufficient for the convergent series solutions.

4 Entropy generation

This sector is associated with the influence of MHD Prandtl fluid with heat transfer on entropy generation. Local volumetric rate of entropy generation is defined as

$$S_{gen}''' = \frac{k}{T_\infty^2}\left[\left(\frac{\partial T}{\partial y}\right)^2 + \frac{16\sigma^* T_\infty^3}{3k^*}\left(\frac{\partial T}{\partial y}\right)^2\right] + \frac{\sigma B_0^2 u^2}{T_\infty} + \frac{D_m}{T_\infty}\left(\frac{\partial T}{\partial y}\frac{\partial C}{\partial y}\right)$$

$$+ \frac{\mu}{T_\infty}\left[\frac{A}{C}\left(\frac{\partial u}{\partial y}\right)^2 + \frac{A}{6C^3}\left(\frac{\partial u}{\partial y}\right)^4\right] + \frac{D_m}{C_\infty}\left(\frac{\partial C}{\partial y}\right)^2. \tag{18}$$

Above equation is the combination of three different phenomena. First is heat transfer, second due to magnetic field and third one is due to viscous dissipation of Walter's B fluid. Characteristics entropy generation rate is defined as

$$\dot{S}_0''' = \frac{k(\Delta T)^2}{l^2 T_\infty^2}, \tag{19}$$

Thus, the dimensionless form of entropy generation is obtained by taking ratio of Eqs. (21) and (22).

$$N_G = \frac{S_{gen}'''}{\dot{S}_0'''} = \mathrm{Re}\left[\left(1 + \frac{4}{3}R\right)\theta''\right] + \frac{1}{\theta_f^2}\mathrm{Re}\,Br\,M f'^2$$

$$- \frac{1}{\theta_f^2}\mathrm{Re}\,Br\left[\alpha f''^2 + \beta f''^4\right] + \Lambda\mathrm{Re}\left(\frac{1}{\theta_f}\phi'^2 + \phi'\theta'\right). \tag{20}$$

where $\mathrm{Re} = \frac{U_w(x,t)x}{\upsilon}$, $Br = \frac{\mu(U_w(x,t))^2}{k\Delta T}$ $\Lambda = \frac{D_m T_\infty}{k}\left(\frac{\Delta C}{\Delta T}\right)$ and $\theta_f = \frac{\Delta T}{T_\infty}$.

5 Results and discussion

Analysis and physical significance of Prandtl fluid parameters, unsteadiness parameter, radiation parameter, thermal and concentration Biot numbers, Prandtl number, Eckert number, Schmidt number and Soret and Dufour analysis. Figure 4 shows the plot of velocity profile $f'(\eta)$ for different values of unsteadiness parameter ϵ. It is clear from this Fig. that ϵ decreases the velocity profile. Physically an increase of time offers larger resistance to the flow which reduces the velocity field. The influence of Prandtl fluid parameters α and β is shown in Figs. 5 and 6. It is seen that velocity enhances throughout the domain with increasing values of α and β. The momentum boundary layer also boost. Figure 7 shows the outcome of the mixed convection parameter on the velocity profile. Greater values of mixed convection parameter growths the velocity profile. Figure 8 represents the impact of the ratio of concentration and buoyancy force. For larger values of N^* the velocity field enhanced. Larger values of M decays the velocity profile and boundary layer thickness. Because the growth in M corresponds to the increase in Lorentz force which creates the resistance in fluid flow, thus velocity reduces (see Fig. 9). While the opposite behavior is observed in Fig. 10. For the larger values of M. Figure 11 illustrates that temperature distribution is boosting the function of the unsteadiness parameter. This is since the rate of heat transfer increases which ultimately enhances the temperature boundary layer. Figure 12 display the increasing behavior of the concentration field for different values of ϵ. Figure 13 indicates that the temperature enhances for larger β. Figure 14 captures the impact of R on the temperature field. Temperature boost with increasing value of R. Rate of heat transfer at the boundary layer region also increases. Figures 15, 16, 17, 18 are presented to compare the effects of Biot numbers on the temperature and concentration fields respectively. Temperature boundary layer is an raising function of Bi_1 and Bi_2. Figures 19 and 20 depict the Soret ("thermophoresis") and Dufour ("diffusion thermo") impacts on the temperature and concentration distributions. The values of Soret/Dufour effects are taken in such a way that their product is constant so that the mean temperature remains constant as well. The Dufour number Du (which indicates the energy flux due to mass concentration gradient) is increased for larger values of temperature and smaller values of Soret number Sr (which generates mass flux due to temperature gradient). Thus it enhances the energy flux due to mass transfer rate and mass flux which significantly increases the temperature. The reverse behavior of Sr and Du is noticed in Fig. 20. Figure 21 elucidates variation of Prandtl number ("ratio of momentum diffusivity to the thermal diffusivity") on dimensionless temperature distribution $\theta(\eta)$. For larger values of Prandtl number the thermal diffusivity decreases and thus both temperature and thermal boundary layers are reduced. Figure 22 shows the influence of the concentration field on the Prandtl number. It shows monotonic behavior on $\phi(\eta)$. Prandtl number increases the concentration when it is closer to the sheet but away from the sheet it decreases and asymptotically approaches zero. Figures 23 and 24 discuss the effects of Eckert number on $\theta(\eta)$ and $\phi(\eta)$. Figure 23 reports that with an increase in Eckert number Ec both
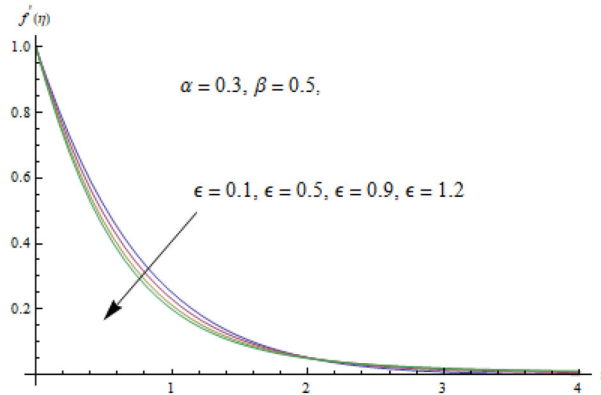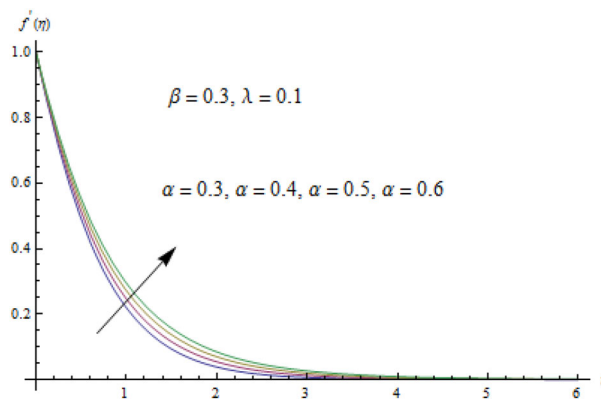
Fig. 4 Impact of ϵ on $f'(\eta)$

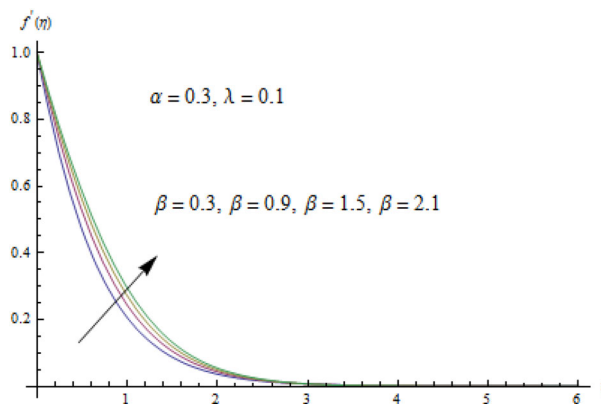**Fig. 5** Impact of α on $f'(\eta)$

Fig. 6 Impact of β on $f'(\eta)$

the temperature and thermal boundary layer thickness is enhanced. Monotonic behavior of the concentration field is noticed for larger values of Ec in Fig. 24. Near the wall it reduces and away from the wall it increases. Figure 25 illustrates the impact of the Schmidt number on $\phi(\eta)$. Concentration field decays when Sc increases.

Figures 26, 27, 28, 30, 31 display the differences of physical parameters on the Nusselt and the Sherwood numbers respectively. Local Nusselt number reduces with an increase in the unsteadiness parameter (see Fig. 26). Figure 27 shows reverse behavior for larger values of R. A small deviation in local Nusselt number is observed for larger values of Eckert number Ec (see Fig. 28). Figures 29 and 30 depict the impact of γ and Sc on the mass transfer rate. An increase in ϵ and Sr decreases the mass transfer rate at the surface. Figure 31 shows increasing behavior for Sherwood number when concentration Biot number is increased.
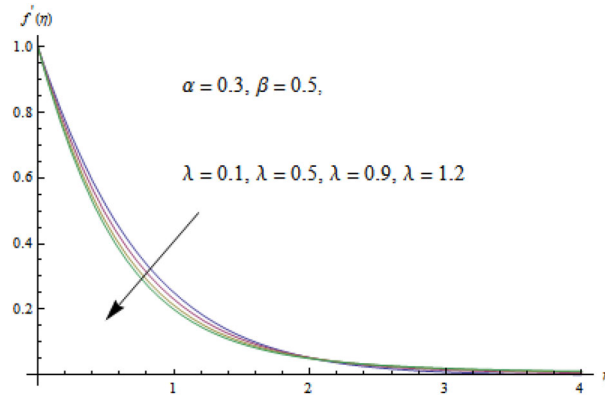
Fig. 7 Impact of λ on $f'(\eta)$
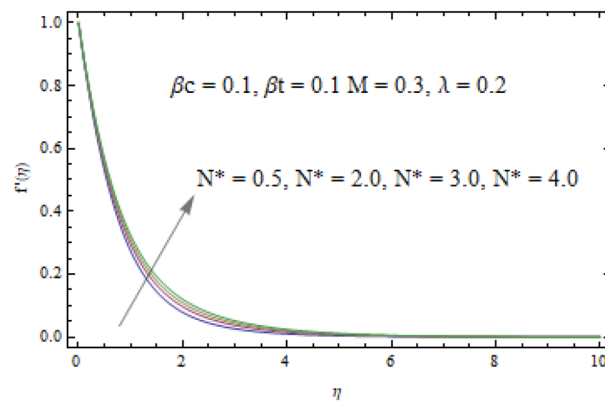
Fig. 8 Impact of N^* on $f'(\eta)$
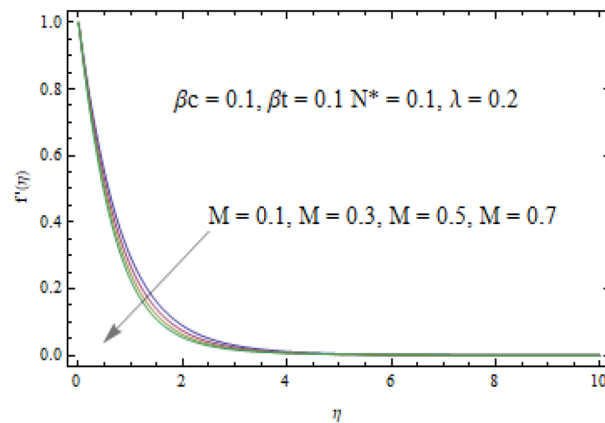
Fig. 9 Impact of M on $f'(\eta)$

Figures 32 and 33 show the flow behavior of fluid parameter, no increment is observed near the wall but far away from the wall entropy generation increases rapidly for greater values of α and β. The dispersion of M on the entropy generation is displayed in Fig. 34. Magnetic parameter persuade Lorentz force which boost the entropy generation. The deviation of entropy generation with η is depicted in Fig. 35 for diverse values of radiation parameter. An increase in radiation parameters leads to an increase in entropy generation. It is also detected that near the surface variation is almost negligible. Variation of entropy generation with Reynolds number is discussed in Fig. 36. It is noted that the entropy generation rises with larger Reynolds number, because larger Reynolds number corresponds to the larger inertia and smaller viscous force. The effect of
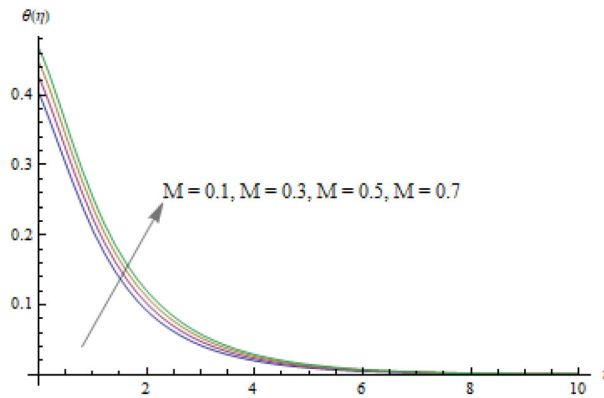
Fig. 10 Impact of M on $\theta(\eta)$
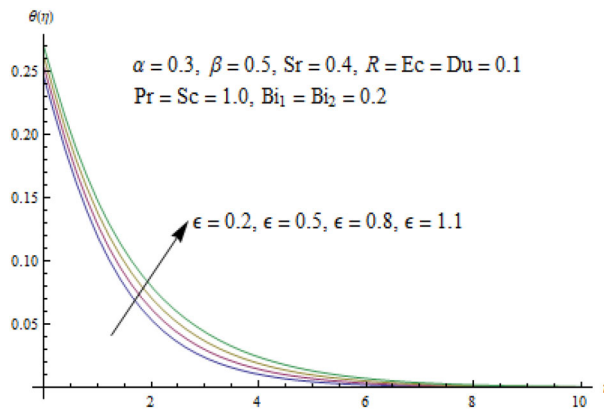
Fig. 11 Impact of ϵ on $\theta(\eta)$
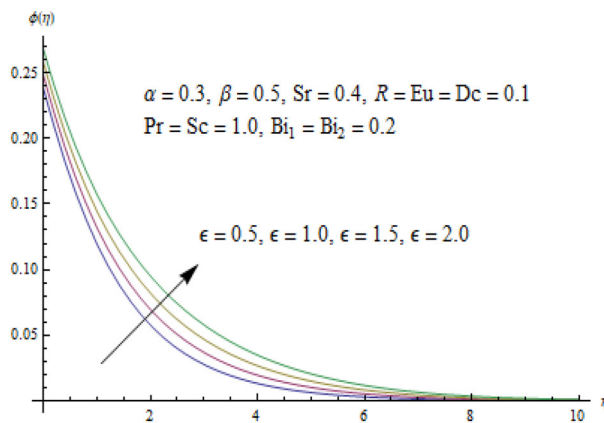
Fig. 12 Impact of ϵ on $\phi(\eta)$

θ_f on the entropy generation is display in Fig. 37. It is understood from this Fig. that entropy generation is decreased when the temperature ratio parameter enhances. The effect of Brickman number is discus in Fig. 38. Brickman number produced heat transport by viscous heating, which improves in entropy generation.

Table 2 investigates the variations of Prandtl fluid and unsteadiness parameters on the skin friction coefficient.The destructive values of the skin-friction coefficient revenues that the surface applies a drag force on the fluid. The amount of the skin-friction coefficient is enlarged for greater values of α, β and ϵ (Tables 2). Tables 3 shows the comparison between the results. We found good comparison for different values of Biot number when Pr = 0.72.

$\theta(\eta)$

$\alpha = 0.3, \lambda = 0.1, Sr = 0.4, R = Ec = Du = 0.1$
$Pr = Sc = 1.0, Bi_1 = Bi_2 = 0.2$

$\beta = 1.0, \beta = 4.0, \beta = 5.0, \beta = 6.0$

Fig. 13 Impact of β on $\theta(\eta)$

$\theta(\eta)$

$\alpha = 0.3, \beta = 0.5, \lambda = Ec = Du = 0.1, Sr = 0.4$
$Pr = Sc = 1.0, Bi_1 = Bi_2 = 0.2$

$R = 0.1, R = 0.2, R = 0.3, R = 0.4$

Fig. 14 Impact of R on $\theta(\eta)$

$\theta(\eta)$

$\alpha = 0.3, \beta = 0.5, \lambda = Ec = Du = 0.1, Sr = 0.4$
$Pr = Sc = 1.0, Bi_2 = 0.2$

$Bi_1 = 0.3, Bi_1 = 0.4, Bi_1 = 0.5, Bi_1 = 0.6$

$\theta'(\eta)$

$Bi_1 = 0.3, Bi_1 = 0.4, Bi_1 = 0.5, Bi_1 = 0.6$
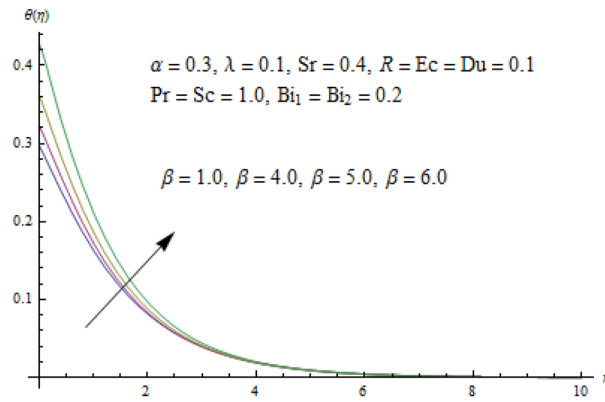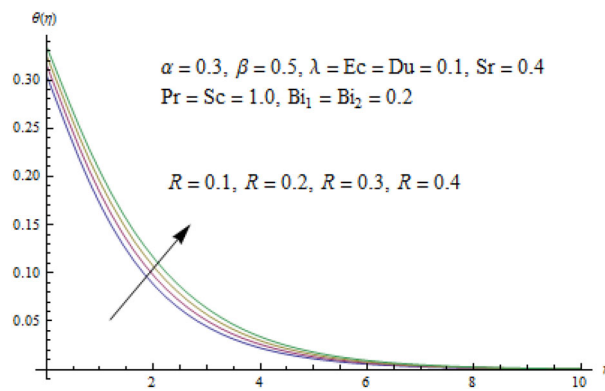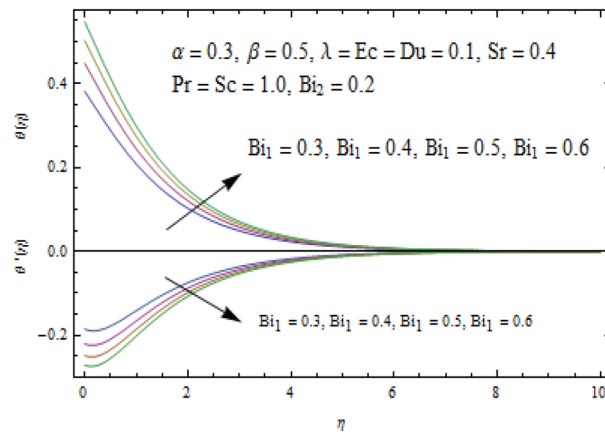
Fig. 15 Impact of Bi_1 on $\theta(\eta)$ and $\theta'(\eta)$
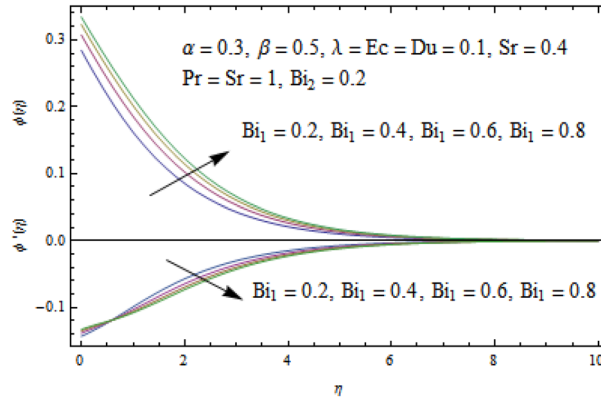
Fig. 16 Impact of Bi_1 on $\phi(\eta)$ & $\phi'(\eta)$
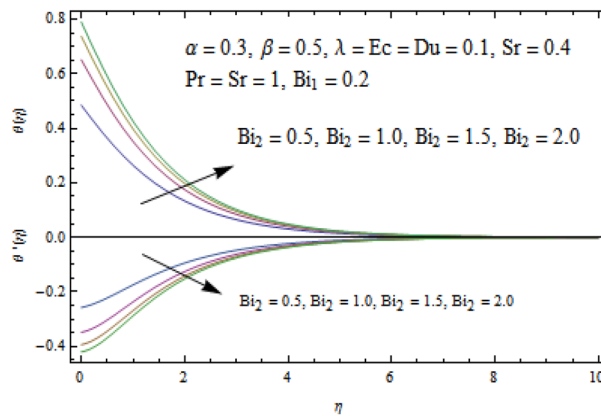
Fig. 17 Impact of Bi_2 $\theta(\eta)$ & $\theta'(\eta)$
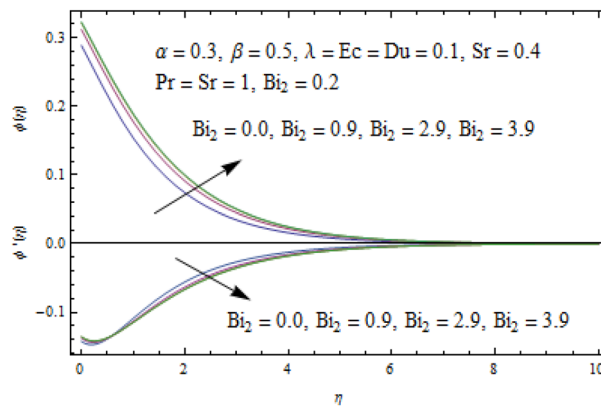
Fig. 18 Impact of Bi_2 on $\phi(\eta)$ and $\phi'(\eta)$

6 Conclusions

Radiative flow of MHD Prandtl fluid with nonlinear mixed convection, entropy generation and convective heat and mass conditions, over an unsteady stretching sheet is examined. The main observations are summarized through the following points.

- Velocity field $f'(\eta)$ increases for larger values of Prandtl fluid parameters α and β.
- Unsteady parameter λ reduces the velocity throughout the region whereas opposite behavior is observed for the temperature and concentration profiles.
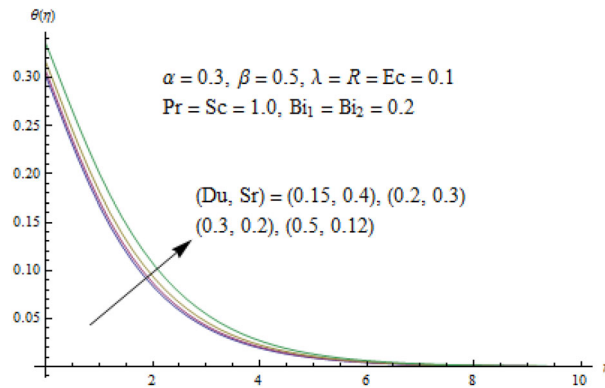
Fig. 19 Impact of *Du* and *Sr* on $\theta(\eta)$
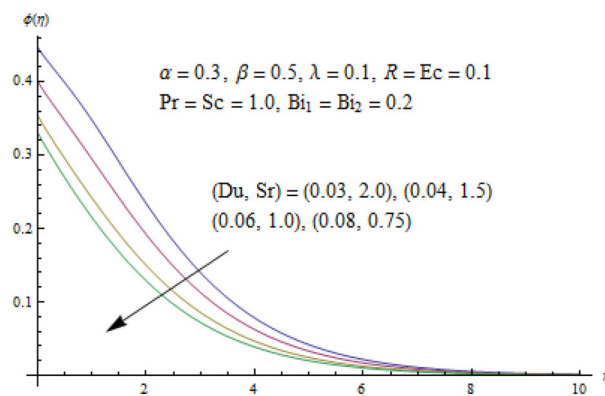
Fig. 20 Impact of (Du, Sr) on $\phi(\eta)$
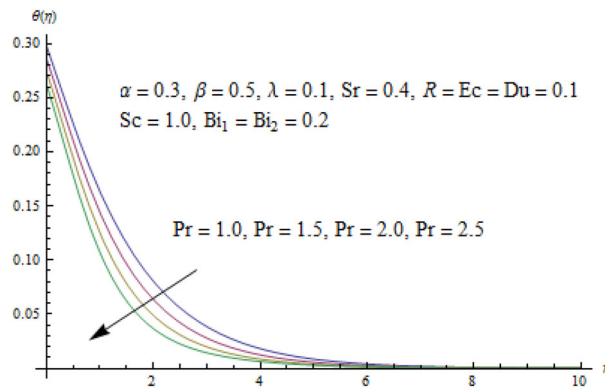
Fig. 21 Impact of Pr on $\theta(\eta)$

- Parameter β enhances the temperature and thermal boundary layer thickness.
- The temperature profile shows increasing behavior for larger values of radiation parameter R.
- The temperature field increases when Eckert number is in strength.
- The effects of Soret and Dufour on the thermal and concentration distributions are practically opposite.
- Thermal and concentration Biot numbers boost the temperature and concentration profiles.
- Prandtl and Eckert numbers have monotonic behavior on the concentration field.
- The concentration field decreases for larger values of Schmidt number Sc.
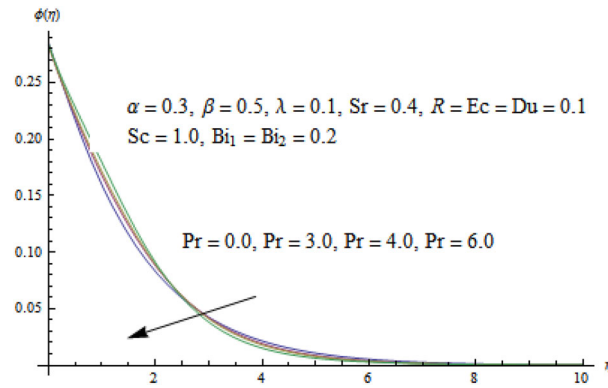
Fig. 22 Impact of Pr on $\phi(\eta)$
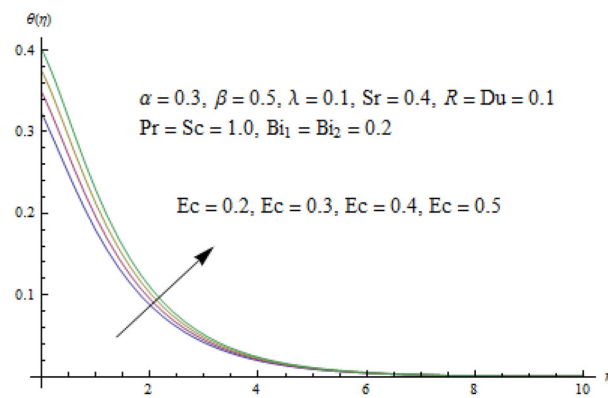
Fig. 23 Impact of and Ec $\theta(\eta)$
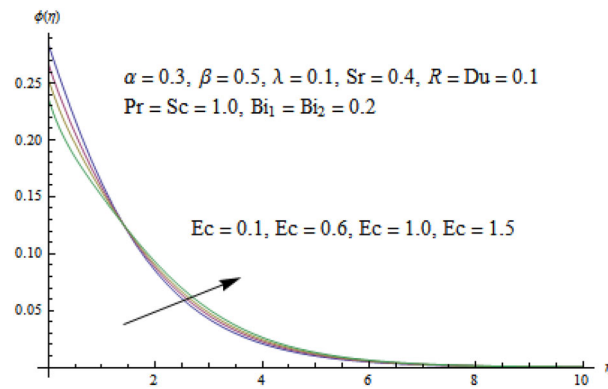
Fig. 24 Impact of Ec on $\phi(\eta)$

- The skin friction coefficient is boosted for increasing values of α, β and λ.
- Prandtl fluid parameters enhance the entropy generation rate.
- Entropy generation increase with magnetic parameter, Reynolds number and Brinkman number, while reverse behavior is observed for larger values of radiation parameter, temperature ratio parameter.
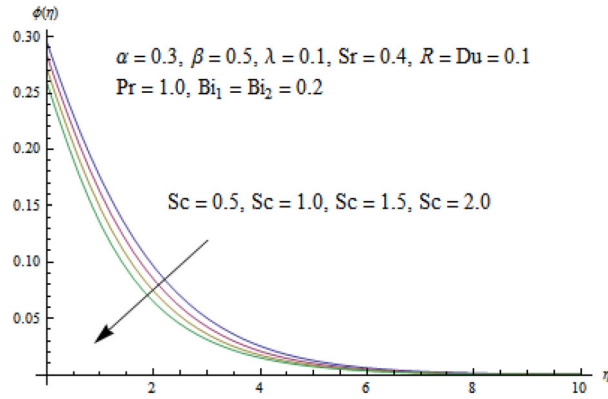
Fig. 25 Impact of *Sc* on $\phi(\eta)$
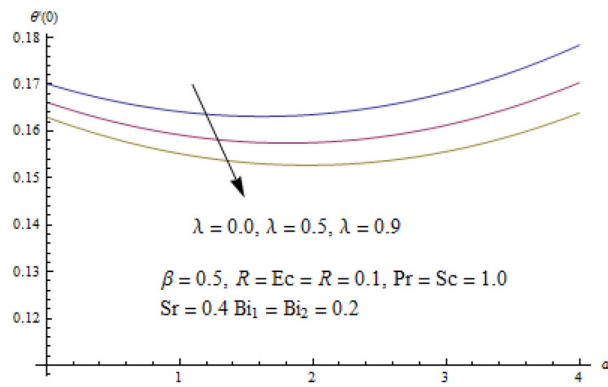
Fig. 26 Impact of λ on $\theta'(0)$
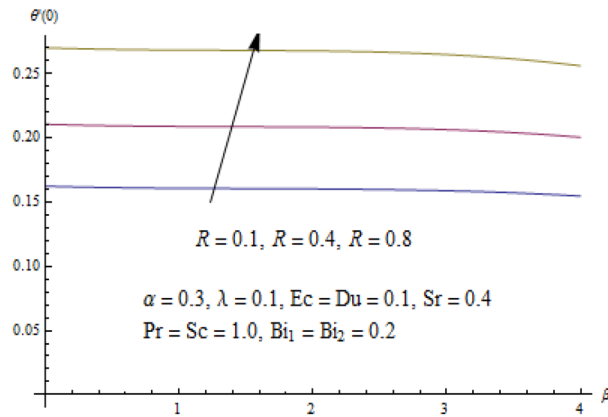
Fig. 27 Impact of *R* on $\theta'(0)$
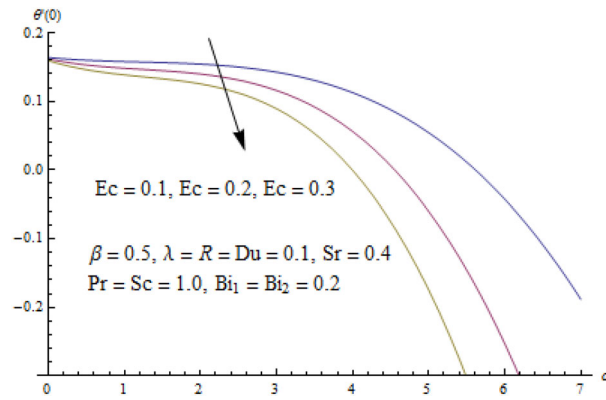
Fig. 28 Impact of Ec on $\theta'(0)$
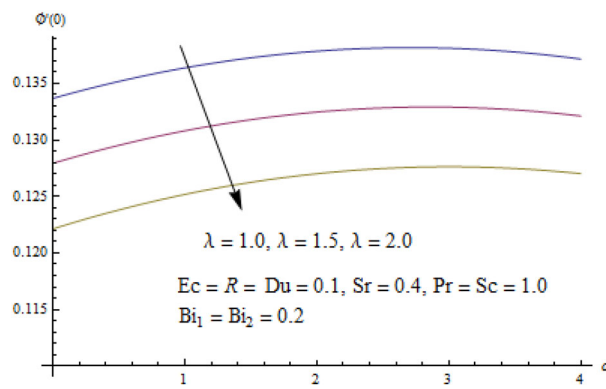
Fig. 29 Impact of λ on $\phi'(0)$
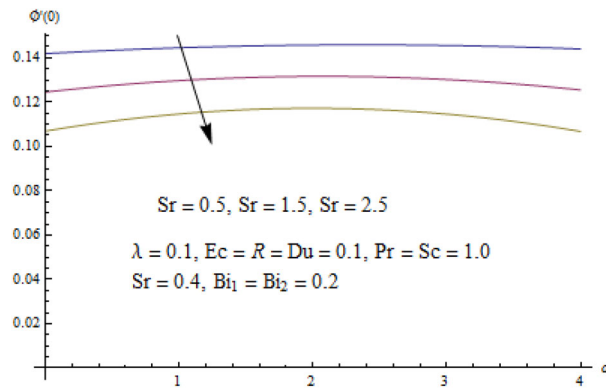
Fig. 30 Impact of Sr on $\phi'(0)$
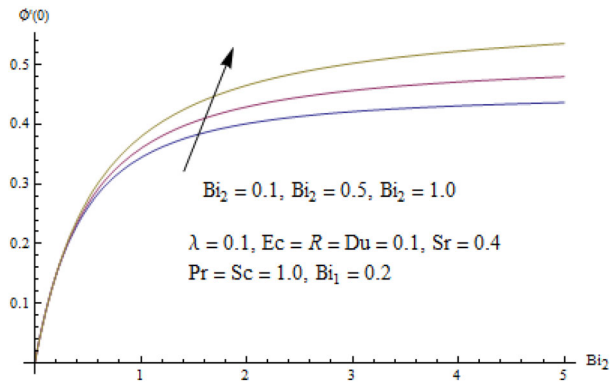
Fig. 31 Impact of Bi_2 on $\phi'(0)$
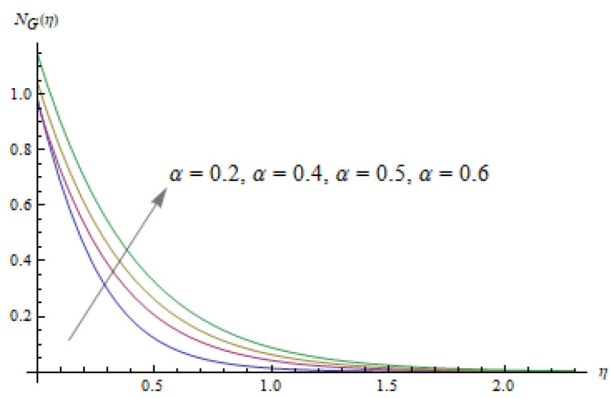
Fig. 32 Impact of α on $N_G(\eta)$
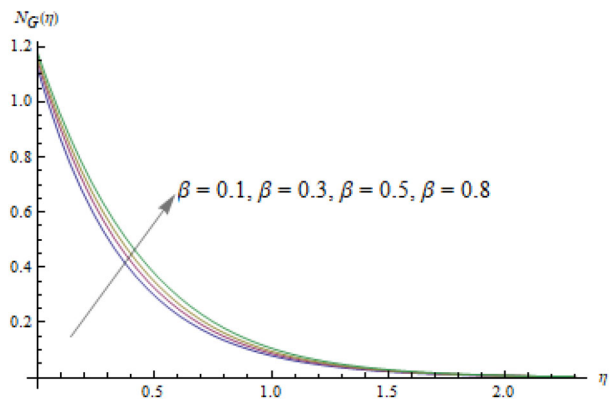
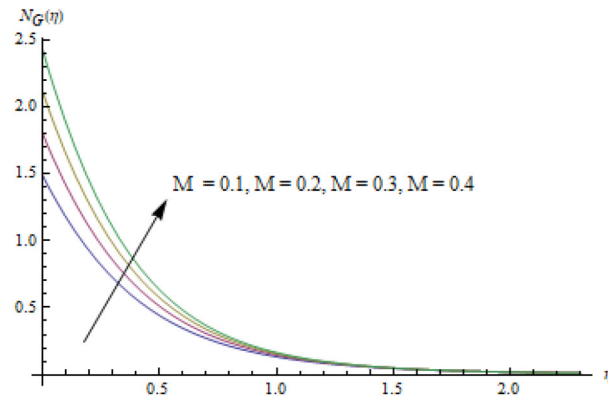**Fig. 33** Impact of β on $N_G(\eta)$
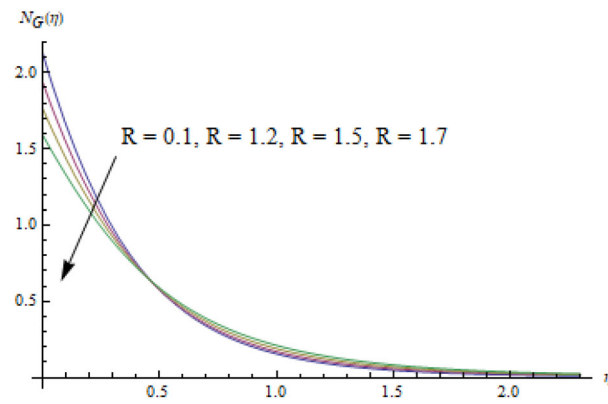
Fig. 34 Impact of M on $N_G(\eta)$

Fig. 35 Impact of R on $N_G(\eta)$
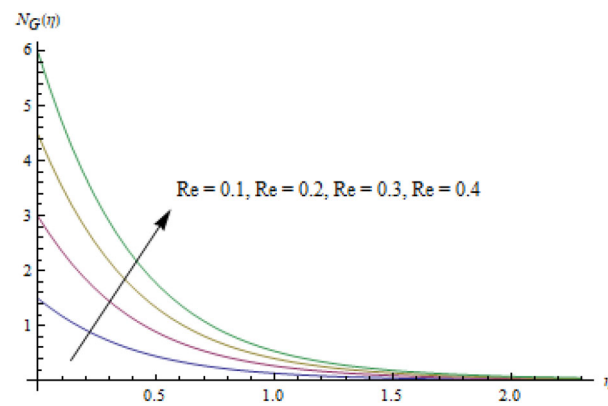
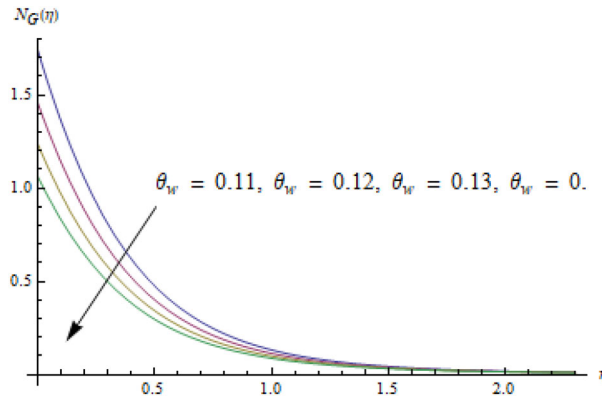**Fig. 36** Impact of Re on $N_G(\eta)$
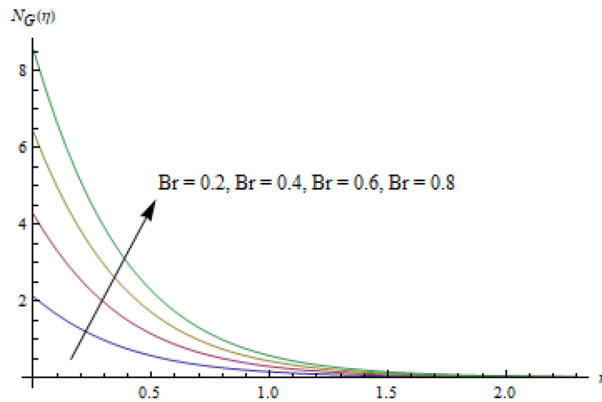
Fig. 37 Impact of θ_w on $N_G(\eta)$

Fig. 38 Impact of B_r on $N_G(\eta)$

Table 2 Values of skin-friction coefficient $\frac{1}{2}Re_x^{1/2}C_{f_x}$ for different parameters

λ	α	β	$-\frac{1}{2}Re_x^{1/2}C_{f_x}$
0.1	0.3	0.5	0.7159
0.2			0.7422
0.25			0.7555
0.35			0.7820
	0.35		0.7202
	0.4		0.7729
	0.45		0.8008
		0.6	0.7335
		0.7	0.7495
		0.8	0.7641

Table 3 Comparison with Aziz [6], Ishak [18] and Makinde & Olanrewaju [23] for (incompressible fluid) -3b8'(0) when Pr = 0.72

Bi_1	Aziz [6]	Ishak [18]	Makinde and Olanrewaju [23]	$-\theta'(0)$
0.05	0.0428	0.0428	0.0428	0.042
0.1	0.0747	0.0747	0.0747	0.0728699
0.2	0.1193	0.1193	0.1193	0.111448
0.4	0.1700	0.1700	0.1700	0.167411
0.6	0.1981	0.1981	0.1981	0.19026
0.8	0.2159	0.2159	0.2159	0.210779

Declarations

Conflict of interest The authors declare that there is no conflict of interest.

References

1. Adelaja, A.O.; Dirker, A.J.; Meyer, P.: Experimental study of entropy generation during condensation in inclined enhanced tubes. Int. J. Multiphase Flow **145**, 103841 (2021)
2. Afilal, M.; Alahyane, M.; Soufyana, A.: Uniform decay rates of a caupled suspension bridges with temperature. Arbian J. Math. **10**, 505–511 (2021)
3. Akbar, N.S.; Khan, Z.H.; Haq, R.U.; Nadeem, S.: Dual solutions in MHD stagnation-point flow of Prandtl fluid impinging an shrinking sheet. Appl. Math. Mech. Engl.-Ed 35, 813-820 (2014). Entropy
4. Akbar, Y.; Abbasi, F.M.: Impact of variable viscosity on peristaltic motion with entropy generation. Int. Comm. Heat Mass Transfer. **118**, 104826 (2020)
5. Ali, I.; Haq, S.K.; Nisar, S.; Arifeen, S.: UI: numerical study of 1D and 2D dvection–diffusion–reaction equations using Lueas and Fibonacci polynomials. Arbian J. Math. **10**, 513–526 (2021)
6. Aziz, A.: A similarity solution for laminar thermal boundary layer over a flat plate with a convective surface boundary condition. Commun. Nonlinear Sci. Numer. Simul. **14**, 1064–1068 (2009)
7. Balazadeh, N.; Sheikholeslami, M.; Ganji, D.D.; Li, Z.: Semi analytical analysis for transient Eyring-Powell Squeezing flow in a stretching channel due to magnetic field using DTM. J. Mol. Liq. **260**, 30–36 (2019)
8. Balazadeh, N.; Sheikholeslami, M.; Ganji, D.D.; Li, Z.: Semi analytical analysis for transient Eyring-Powell Squeezing flow in a stretching channel due to magnetic field using DTM. J. Mol. Liq. **260**, 30–36 (2019)
9. Bhattacharyya, K.: Heat transfer analysis in unsteady boundary layer stagnation-point flow towards a shrinking/streching sheet. Ain Shams Eng. J. **4**, 259–264 (2013)
10. Eid, R.M.; Mohny, K.L.; Al Hossany, A.F.: Homogeneous-heteroggeneous catalysis on electromagnetie radiative Prandtl fluid flow: Darcy–Forchheimer substance scheme. Surface and Interfaces **24**, 101119 (2021)
11. Haddadou, H.: H-convergence of a class of quasilinear equations in perforated domains beyond periodic setting. Arbian J. Math. **10**, 91–101 (2021)
12. Hayat, T.; Mustafa, M.; Pop, I.: Heat and mass transfer for Soret and Dufour effect on mixed convection boundary layer flow over a stretching vertical surface in a porous medium filled with a viscoelastic fluid. J. Commun. Nonlinear Sci. Numer. Simul. **15**, 1183–1196 (2010)
13. Hayat, T.; Safdar, A.; Awais, M.; Mesloub, S.: Soret and Dufour effects for three dimensional flow in a viscoelastic fluid over a stretching surface. Int. J. Heat Mass Transfer. **55**, 2129–2136 (2012)
14. Hayat, T.; Naz, R.; Asghar, S.; Alsaedi, A.: Soret and Dufour effects on MHD rotating flow of a viscoelastic fluid. Int. J. Numer. Methods Heat Fluid Flow **24**, 498–520 (2014)
15. Hayat, T.; Asad, S.; Mustafa, M.; Alsaedi, A.: Radiation effects on the flow of Powell–Erying fluid past an unsteady inclined stretching sheet with non-uniform heat source/sink. Plos One **9**, e103214 (2014)
16. Hayat, T.; Qayyum, S.; Waqas, M.; Ahmed, B.: Influence of thermal radiation and chemical reaction in mixed convection stagnation point flow of Carreau fluid. Result Phys. **7**, 4058–4064 (2017)
17. Hayat, T.; Sajjad, Lahiba; Khan, I.M.; Khan, M.I.; Alsaedi, A.: Salient aspects of thermos-diffusion and diffusion thermos on unsteady dissipative flow with entropy generation. J. Mol. Liq. **282**, 557–565 (2019)
18. Ishak, A.: Similarity solutions for flow and heat transfer over a permeable surface with convective boundary condition. Appl. Math. Comput. **217**, 837–842 (2010)
19. Khan, M.I.; Khan, S.A.; Hayat, T.; Khan, M.I., Alsaedi, A.: Nanomaterial based flow of Prandtl-Eyring (non-Newtonian) fluid using Brownian and thermophoretic diffusion with entropy generation. Comp. Meth. Prog. Biomed. **180**, 105017 (2019)
20. Khan, S.A.; Hayat, T.; Alsaedi, A.: Numerical study for entropy optimized radiation unsteady flow of Prandtl liquid. Fuel **319**, 123601 (2022)
21. Lin, Y.; Zheng, L.; Chen, G.: Unsteady flow and heat transfer of pseudo-plastic nanoliquid in a finite thin film on a stretching surface with variable thermal conductivity and viscous dissipation. Powder Technol.. **274**, 324–332 (2015)
22. Lin, Y.; Zheng, L.; Zhang, X.; Ma, L.; Chen, G.: MHD pseudoplastic nanofluid unsteady flow and heat transfer in a finite thin film over stretching surface with internal heat generation. Int. J. Heat Mass Transf. **84**, 903–911 (2015)
23. Makinde, O.D.; Olanrewaju, P.O.: Buoyancy effects on thermal boundary layer over a vertical plate with a convective surface boundary condition. ASME J. Fluid Eng. **132**, 1–4 (2010)
24. Mukhopadhyay, S.: Diffusion of chemically reactive species in Casson fluid flow over an unsteady permeable stretching surface. J. Hydrodyn. **25**, 591–598 (2013)

25. Mukhopadyay, S.; Bhattacharyya, K.; Layek, G.C.: Casson fluid flow over an unsteady stretching surface. Ain Shams Eng. J. **4**, 933–938 (2013)
26. Reddy, M.G.: Unsteady radiative–convective boundary-layer flow of a Casson fluid with variable thermal conductivity. J. Eng. Phys. Thermophys. **88**, 1187–5 (2015)
27. Rosca, N.C.; Pop, I.: Unsteady boundary layer flow over a permeable curved stretching/shrinking surface. Eur. J. Mech. B/Fluids **51**, 61–67 (2015)
28. Safarzadeh, S.; M. Azodi, N. A.; Aldaghi, A.; Tahri, M.; Fard P.; Mohammadi, M.: Energy and entropy generation analysis of a nanofluid-based helically coiled pipe under a constant magnetic field using smooth and microfin pipe: Experimental study and prediction via ANFIS model. Int. Comm. Heat Mass Transfer, 126, 105405 (2021)
29. Samal, S.K.; Moharana, M.K.: Second law analysis of recharging microchannel using entropy generation minimization method. Int. J. Mech. Sci. **193**, 106174 (2021)
30. Sec, Y.S.; Leong, K.C.: Entropy generation for flow boiling on a single semi-circular minichannel. Int. J. Heat Mass Transfer **154**, 119689 (2020)
31. Tsai, R.; Huang, J.S.: Heat and mass transfer for Soret and Dufour effects on Hiemeng flow through porous medium onto a stretching surface. Int. J. Heat Mass Transf. **52**, 2399–2406 (2009)
32. Vedavathi, N.; Ramakrishna, K.; Reddy, K.J.: Radiation and mass transfer effects on unsteady MHD convective flow past an infinite vertical plate with Dufour and Soret effect. Ain Shams Eng. J. **6**, 363–371 (2015)
33. Wang, J.; Yang, M.; Zhang, Y.: Onset of double-diffusive convection in horizontal cavity with Soret and Dufour effects. Int. J. Heat Mass Transf. **78**, 1023–1031 (2014)
34. Zheng, L.; Wang, L.; Zhang, X.: Analytic solutions of unsteady boundary flow and heat transfer on a permeable stretching sheet with non-uniform heat source/sink. Commun. Nonlinear Sci. Numer. Simul. **16**, 731–740 (2011)
35. Zheng, L.C.; Jin, X.; Zhang, X.X.; Zhang, J.H.: Unsteady heat and mass transfer in MHD flow over an oscillatory stretching surface with Soret and Dufour effects. Acta Mech. Sinica. **29**, 667–675 (2013)